Materials Letters 305 (2021) 130743

Contents lists available at ScienceDirect

Materials Letters

journal homepage: www.elsevier.com/locate/matlet

In-situ heating effect of laminar plasma jet during Mo coatings deposition

Hui-Yu Zhang, Sen-Hui Liu, Chang-Jiu Li, Cheng-Xin Li *

State Key Laboratory for Mechanical Behavior of Materials, School of Materials Science and Engineering, Xi'an Jiaotong University, Xi'an, Shaanxi 710049, China

ARTICLE INFO

Keywords:
Microstructure
Thick films
Wear and tribology

ABSTRACT

Laminar plasma has the characteristics of a long plasma jet, low velocity, and high temperature, which make it able to cover and heat the substrate during the spraying process. The results show that when the standoff distance is short, the coating is strengthened by in-situ heating of the plasma jet and shows higher erosion resistance at high erosion angles and bulk-like material tendency. When the standoff distance is long, the substrate temperature is low, the coating shows higher erosion resistance at a lower erosion angle.

1. Introduction

Laminar plasma is another working state of direct current arc plasma, which is obtained by optimizing the flow channel of the plasma torch and reducing the flow rate of working gas [1–3]. Its main characteristics are longer plasma jet length, lower velocity, higher temperature, lower axial velocity and temperature gradient, due to less air engulfment [1–6]. The differences between turbulent plasma spray and laminar plasma spray are mainly because of the longer heating time of particles [4,5,7]. However, the heat input of the long laminar plasma jet may also affect the properties of the coatings.

From previous experiments [8,9], we know that the laminar plasma can heat the substrate in situ in a short standoff distance, and the deposition state (heating and acceleration) of particles will not change much with the spraying distance [5,8,9]. Therefore, the heating process of the substrate can be controlled by changing the position of the substrate (standoff distance). To control the temperature of the substrate, we decrease the standoff distance to realize the in-situ heating to the substrate.

2. Material and methods

Commercial sintered molybdenum powder (140/325 mesh, MA9900, Höganäs China, Mo $\geq$ 99.5%) was used. The average diameter is 77 μm (d_{10} = 52 μm, d_{90} = 112 μm). The main variable is the standoff distance, and the substrate will be only heat by the plasma jet without any other heat source. The erosion performance is also measured by a self-designed blast erosion tester [10]. The average mass loss of later 5 erosion tests was used to represent the erosion resistance of the coating. Schematic diagrams and detailed parameters used are shown in Fig. 1. And the details about the equipment are listed in the Electronic Supplementary Information document.

3. Results and discussion

The local temperature of the substrate, the moment of the plasma jet swept, in condition A is about 600 °C (Supplementary Fig. 2). The coatings obtained at 100 mm are marked as A and the others are marked as B. Fig. 2(a)–(d) shows the surface morphology, fracture, the polished cross section, and the surface morphology of coating A. Since the length of the plasma jet is long enough to cover the substrate, the coating surface will be heated in-situ. The deposition rate based on the thickness and number of the cycles is about 28 μm/cycle for A and 17 μm/cycle for B. The surface of the coatings is not even, and some small protrusions are located on the surface (Fig. 2a). The surface roughness of the coatings (Ra) is about 29 μm. From Fig. 2 (b), the protrusions show a cauliflower-like shape tendency, and the whole surface is covered by a thin furry-like structure. From the fractured view of the coating (Fig. 2c), an obvious lamellar structure can be observed. From the cross-sectional view (Fig. 2d), the two-dimensional unbonded interface between the splats is not obvious, indicating that diffusion may occur under the effect of the in-situ heating by the plasma jet, which improves the bonding between the lamellae. Besides, the pores are mostly periodically gathered spherical pores. Fig. 2 (e) - (h) shows the microstructure of coating B. The results show that the surface of the coating is flat, and the roughness is about 21 μm (Fig. 2e). No obvious protrusions can be observed (Fig. 2e). The lamellar structure can be observed in both the fracture (Fig. 2g) and the polished cross section (Fig. 2h), and two-dimensional

* Corresponding author.
E-mail address: licx@mail.xjtu.edu.cn (C.-X. Li).

https://doi.org/10.1016/j.matlet.2021.130743
Received 4 July 2021; Received in revised form 18 August 2021; Accepted 20 August 2021
Available online 25 August 2021

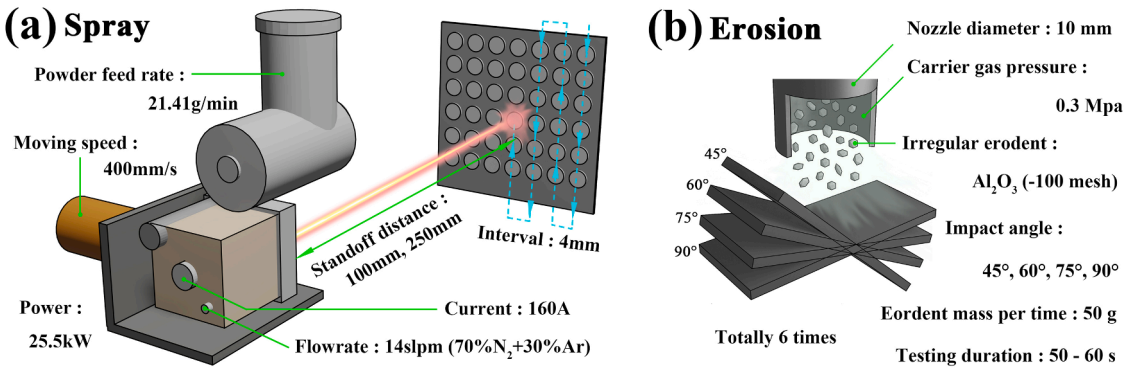

Fig. 1. The schematic diagram of (a) the spraying process and (b) the erosion test.

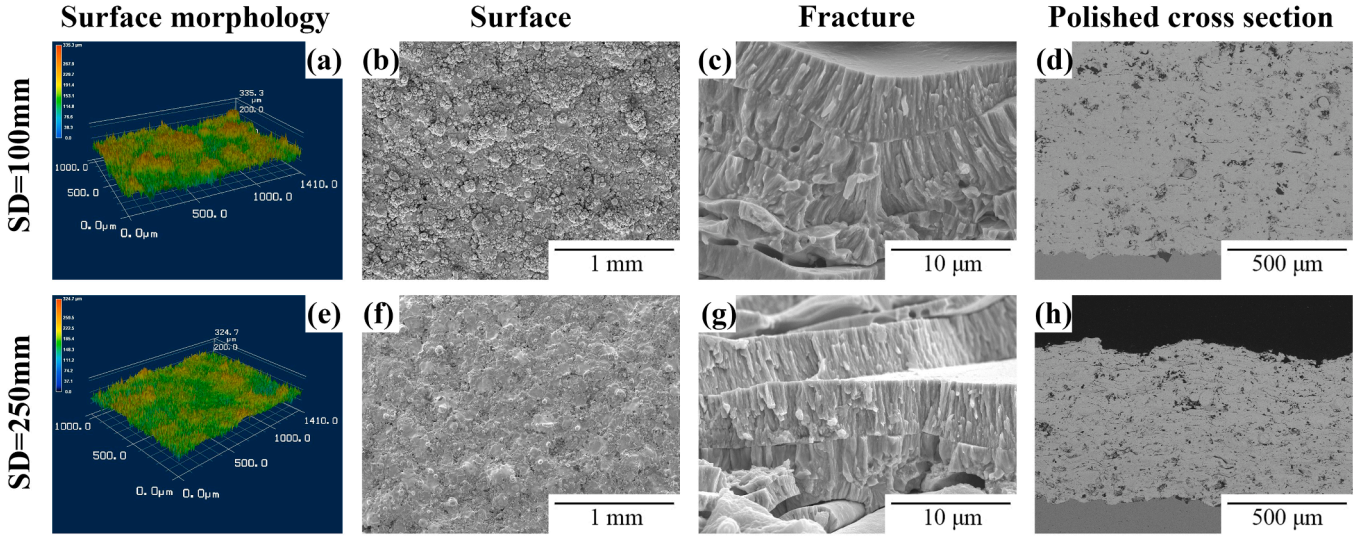

Fig. 2. Microstructure of plasma sprayed Mo coating.

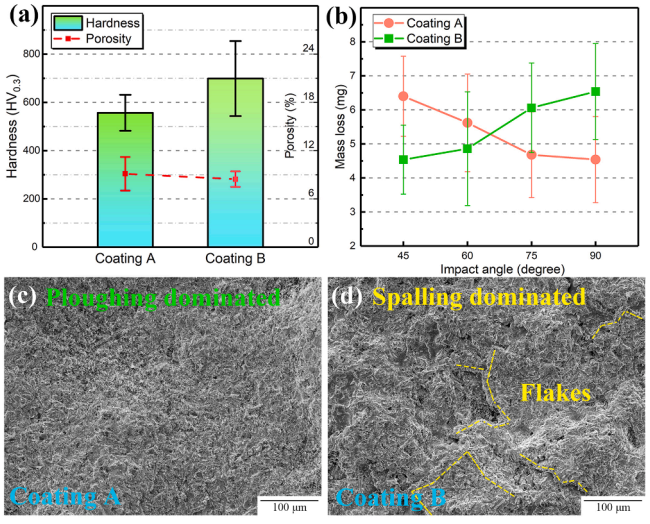

Fig. 3. (a) the hardness and porosity of the coatings, (b) erosion mass loss of the coatings, (c) eroded surface of coating A and (d) coating B.

and spherical pores coexist.

The hardness and the porosity are measured, and the results are shown in Fig. 3(a). In this case, the XRD patterns (supplementary Fig. 3) show that both conditions endure oxidations. Generally, when the standoff distance increases, the oxidation becomes severe and the coatings show higher hardness [9]. The fracture toughness of the coatings can be characterized by the following equation [11]:

$$K_{IC} = \delta\left(\frac{E}{H_v}\right)^{\frac{1}{2}}\frac{P}{c^{3/2}}$$

where $\delta = 0.016 \pm 0.004$ is a constant for Vickers indenter. H_v is the Vickers hardness. E is the elastic modulus. c is the crack size after indentation as a function of the peak load P. Among these variables, E can be calculated by the following equation [12]:

$$\frac{b'}{a'} = \frac{b}{a} - \alpha \bullet \frac{H_v}{E}$$

where α is an empirical coefficient equals 0.45. The ratio of the short diagonal b to the long diagonal a at full load is given by the geometry of Knoop indenter and equals to 1/7.11. a' and b' are the long and the short diagonals of the residual impression after removal of load. From the equation of the coatings, c is the key factor influencing K_{IC}, since the change of $(E/H_v)^{1/2}$ is smaller than $c^{3/2}$. The average of c for coating A is 36.47 μm and for coating B is 43.53 μm, which indicates the in-situ heating process may enhance the fracture toughness of the coatings.

The erosion performance is characterized by the mass loss of the coatings during the erosion test. The mass loss of the two coatings is shown in Fig. 3(b). From the erosion behavior of the coatings at different impact angles, it can be concluded that the mass loss of coating A gradually decreases with the increase of the impact angle and shows the

lowest mass loss under the normal impact, indicating a tendency of erosion performance like the bulk materials. While coatings B shows the opposite tendency, which is like the classic brittle material.

Generally, the erosion resistance of the coatings is determined by the combination of the properties of the material and the structure of the coating, such as hardness, toughness, and porosity.

For coating A, the two-dimensional pores in coating A are fewer (Fig. 2d, h) and the fracture toughness is higher than coating B. Therefore, coating A endures less spalling of the flakes when the impact angle is high. And when the impact angle is lower, the micro-plowing process intensifies, and many micro-furrows can be observed on coating A (Fig. 3c). The main mass loss of coating A is due to the plowing of the erosive particles rather than the spalling of flakes, showing a ductile bulk-like performance.

For coating B, besides the micro-furrows, many flakes can be also seen on the surface, and this may be the main reason for the mass loss of coating B. Under the high-frequency cyclic stress induced by the erodent when the impact angle is high, the cracks gradually grew from the surface of the coating. Once the cracks meet together to form a closed circle, all the splats enclosed by the cracks would peel off [13]. When the impact angle is low, the tangential component which leads to the shear force increases. Since the hardness of coating B is high to resist the penetration of the erodent on the surface, the mass loss caused by micro-plowing is not so severe. Besides, the normal impact which causes the peeling-off of the flakes is decreased when the impact angle is lower. Therefore, coating B shows an increasing tendency on mass loss with the impact angle, which is a common phenomenon amongst brittle materials.

4. Conclusion

The long plasma jet can heat the substrate in situ at a short distance. By controlling the heat input to the substrate, coatings with different microstructures and properties can be obtained. Coatings obtained under in-situ heating of the plasma jet show less unbonded interface, lower hardness but higher toughness, and the erosion performance are bulk-like.

CRediT authorship contribution statement

Hui-Yu Zhang: Data curation, Writing - review & editing, Methodology. **Sen-Hui Liu:** Visualization, Investigation. **Chang-Jiu Li:** Resources. **Cheng-Xin Li:** Supervision.

Declaration of Competing Interest

The authors declare that they have no known competing financial interests or personal relationships that could have appeared to influence the work reported in this paper.

Acknowledgement

This work was supported by the Natural Key R&D Program of China (Basic Research Project, Grant No. 2017YFB0306100), and the National Natural Science Foundation of China (Grant NO. 91860114). And special appreciation to Engineer Wang Jin-Xi for devoting himself to the work in XJTU Thermal Spray Lab.

Appendix A. Supplementary data

Supplementary data to this article can be found online at https://doi.org/10.1016/j.matlet.2021.130743.

References

[1] W. Pan, W. Zhang, W. Zhang, C. Wu, Generation of long, laminar plasma jets at atmospheric pressure and effects of flow turbulence, Plasma Chem. Plasma Process. 21 (2001) 23–35, https://doi.org/10.1023/A:1007037327834.
[2] X. Cao, D. Yu, Y. Xiang, J. Yao, J. Miao, Influence of the Laminar Plasma Torch Construction on the Jet Characteristics, Plasma Sci. Technol. 18 (7) (2016) 740–743, https://doi.org/10.1088/1009-0630/18/7/07.
[3] X. Cao, D. Yu, M. Xiao, J. Miao, Y. Xiang, J. Yao, Design and Characteristics of a Laminar Plasma Torch for Materials Processing, Plasma Chem. Plasma Process. 36 (2) (2016) 693–710, https://doi.org/10.1007/s11090-015-9661-6.
[4] S.H. Liu, C.X. Li, L. Li, J.H. Huang, P. Xu, Y.Z. Hu, G.J. Yang, C.J. Li, Development of long laminar plasma jet on thermal spraying process: Microstructures of zirconia coatings, Surf. Coatings Technol. 337 (2018) 241–249, https://doi.org/10.1016/j.surfcoat.2018.01.003.
[5] S.H. Liu, C.X. Li, H.Y. Zhang, S.L. Zhang, L. Li, P. Xu, G.J. Yang, C.J. Li, A novel structure of YSZ coatings by atmospheric laminar plasma spraying technology, Scr. Mater. 153 (2018) 73–76, https://doi.org/10.1016/j.scriptamat.2018.04.022.
[6] W.X. Pan, G. Li, X. Meng, W. Ma, C.K. Wu, Laminar plasma jets: Generation, characterization, and applications for materials surface processing, Pure Appl. Chem. 77 (2005) 373–378, https://doi.org/10.1351/pac200577020373.
[7] S.H. Liu, H.Y. Zhang, Y.P. Wang, G. Ji, L. Li, P. Xu, J.H. Huang, S.L. Zhang, C.X. Li, C.J. Li, Microstructural evolution of alumina coatings by a novel long laminar plasma spraying method, Surf. Coatings Technol. 363 (2019) 210–220, https://doi.org/10.1016/j.surfcoat.2019.02.018.
[8] H.Y. Zhang, C.X. Li, S.H. Liu, L. Li, G.J. Yang, C.J. Li, S.L. Zhang, Splash involved deposition behavior and erosion mechanism of long laminar plasma sprayed NiCrBSi coatings, Surf. Coatings Technol. 395 (2020), https://doi.org/10.1016/j.surfcoat.2020.125939.
[9] H.Y. Zhang, S.H. Liu, C.J. Li, C.X. Li, Deposition and oxidation behavior of atmospheric laminar plasma sprayed Mo coatings from 200 mm to 400 mm under 20 kW: Numerical and experimental analyses, Surf. Coatings Technol. 400 (2020), 126245, https://doi.org/10.1016/j.surfcoat.2020.126245.
[10] C. Zhang, L. Liu, H. Xu, J. Xiao, G. Zhang, H. Liao, Role of Mo on tribological properties of atmospheric plasma-sprayed Mo-NiCrBSi composite coatings under dry and oil-lubricated conditions, J. Alloy. Compd. 727 (2017) 841–850, https://doi.org/10.1016/j.jallcom.2017.08.195.
[11] G.R. Anstis, A critical evaluation of indentation techniques for measuring fracture toughness I direct crack measurements, Transformation 46 (1981) 533–538.
[12] G. Ben Ghorbal, A. Tricoteaux, A. Thuault, G. Louis, D. Chicot, Comparison of conventional Knoop and Vickers hardness of ceramic materials, J. Eur. Ceram. Soc. 37 (6) (2017) 2531–2535, https://doi.org/10.1016/j.jeurceramsoc.2017.02.014.
[13] C.-J. Li, G.-J. Yang, A. Ohmori, Relationship between particle erosion and lamellar microstructure for plasma-sprayed alumina coatings, Wear 260 (11-12) (2006) 1166–1172, https://doi.org/10.1016/j.wear.2005.07.006.